Imaging the Deep Seismic Structure Beneath a Mid-Ocean Ridge: The MELT Experiment

The MELT Seismic Team

The Mantle Electromagnetic and Tomography (MELT) Experiment was designed to distinguish between competing models of magma generation beneath mid-ocean ridges. Seismological observations demonstrate that basaltic melt is present beneath the East Pacific Rise spreading center in a broad region several hundred kilometers across and extending to depths greater than 100 kilometers, not just in a narrow region of high melt concentration beneath the spreading center, as predicted by some models. The structure of the ridge system is strongly asymmetric: mantle densities and seismic velocities are lower and seismic anisotropy is stronger to the west of the rise axis.

As the oceanic plates separate at mid-ocean ridge spreading centers, partial melting of the upwelling mantle creates enough magma to form a layer of basaltic crust 6 to 7 km thick. Seismic reflection and refraction studies have shown that this crust forms within 1 to 2 km of the ridge axis (*1*). A major question has been how melt is transported from the distributed region of melt production in the mantle to such a narrow zone at the axis. The lack of direct observations of the melt production region at depth has led to the development of two classes of models that describe the nature of the mantle upwelling and pressure-release melting beneath spreading centers.

In passive flow models, viscous drag from the separating plates induces a broad zone of upwelling and melt production that may be 100 km or more across. In these models, the melt must migrate horizontally to the ridge axis, despite the tendency of the buoyancy of melt to drive it vertically. Several possible mechanisms for guiding the melt to the ridge axis have been suggested, such as pressure gradients from deformation of the viscous mantle matrix (*2*), anisotropic permeability of the matrix (*3*), or sloping melt channels at the base of the lithosphere (*4*). As little as a few tenths of a percent melt may be present at any one time, as laboratory and numerical experiments indicate that porous flow may be very efficient in extracting melt (*5*).

In dynamic flow models, in contrast, the buoyancy of melt, the reduction in density of the mantle caused by extraction of melt, and lower viscosity in the upwelling zone combine to focus upwelling and melting into a narrow zone, perhaps only a few kilometers across (*6*). Melt transport is primarily vertical, and most of the melting is beneath the axial zone. Several percent melt must be retained in the mantle matrix in the upwelling region to provide the necessary buoyancy and to reduce the viscosity.

When viscous drag forces dominate in passive flow, upwelling should closely follow the ridge geometry. In contrast, when buoyancy forces dominate, in addition to concentrating upwelling into a narrow zone, the convective pattern is likely to break up into a three-dimensional geometry with distinct upwelling centers (*7*). Some investigators have suggested that upwelling is concentrated into diapirlike features distributed at spots along the ridge, even at the fast-spreading, linear East Pacific Rise (EPR) (*8*). If centers of upwelling are present, then melt must be redistributed along the axis at crustal levels (in dikes for example) to produce an oceanic crust that is relatively uniform in thickness.

Another remaining question is the depth extent of melting. The major element composition of mid-ocean ridge basalts (MORBs) indicates that much of the melt production takes place in the spinel peridotite stability field at depths shallower than about 60 km (*9*). However, uranium-series disequilibria and trace element composition suggest that some of the melting occurs in the garnet stability field at depths exceeding 60 km (*10*). In addition, minor amounts

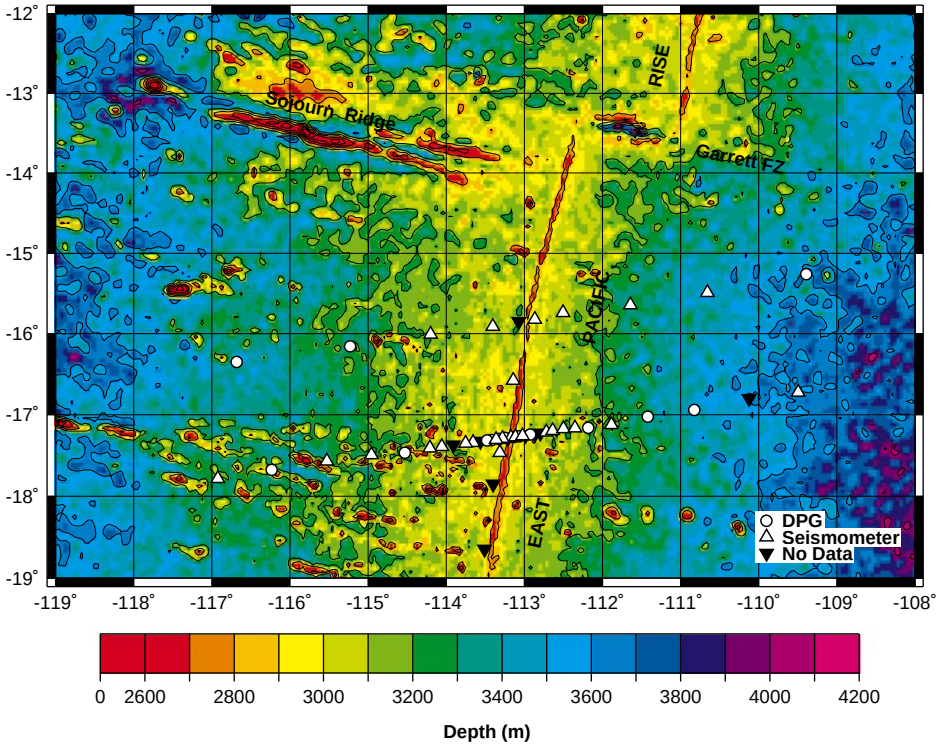

Fig. 1. Locations of ocean-bottom seismometers (OBSs) and bathymetry of the study area. Bathymetry is predicted from dense satellite altimetry and sparse, shipboard bathymetric measurements (*29*). The linear arrays of OBSs were oriented at an angle to the ridge so that they would lie along a great-circle path that includes the seismically active regions bordering the southwest Pacific (Fig. 2). Symbols indicate whether data include three-component seismometer readings (open triangle) or pressure only (open circle), or whether no data were returned (inverted, filled triangle).

D. W. Forsyth* and D. S. Scheirer, Department of Geological Sciences, Brown University, Providence, RI 02912, USA.
S. C. Webb, L. M. Dorman, J. A. Orcutt, A. J. Harding, D. K. Blackman, J. Phipps Morgan, Scripps Institution of Oceanography, University of California, San Diego, La Jolla, CA 92093, USA.
R. S. Detrick, Y. Shen, C. J. Wolfe, J. P. Canales, Woods Hole Oceanographic Institution, Woods Hole, MA 02543, USA.
D. R. Toomey, Department of Geological Sciences, University of Oregon, Eugene, OR 97403, USA.
A. F. Sheehan, Department of Geological Sciences and Cooperative Institute for Research in Environmental Sciences (CIRES), University of Colorado, Boulder, CO 80309, USA.
S. C. Solomon, Department of Terrestrial Magnetism, Carnegie Institution of Washington, Washington, DC 20015, USA.
W. S. D. Wilcock, University of Washington, School of Oceanography, Seattle, WA 98195, USA.

*To whom correspondence should be addressed. E-mail: donald_forsyth@brown.edu

of melting are possible in the presence of water at depths of 150 to 200 km or more (*11*). Because the composition of MORBs and the thickness of the oceanic crust are nearly uniform independent of location of the spreading center, the common view has been that ridges are generally passive features that simply tap a well-stirred, nearly isothermal asthenosphere and that any dynamic upwelling is simply a local response to melting. On the other hand, some investigators have suggested that there is a link between mid-ocean ridges and deep structures in the lower mantle mapped with global seismic tomography (*12*), implying perhaps that upwelling beneath ridges is an active part of a whole-mantle convection system.

The goals of the MELT Experiment are to use seismic and electromagnetic observations to constrain the pattern of upwelling beneath a ridge, the geometry of the region of partial melting, the melt concentration within that region, the distribution of melt within the matrix, and the connectedness of melt pockets. Passive arrays of seismometers, electrometers, and magnetometers were deployed on the sea floor across the EPR to record seismic waves from regional and teleseismic earthquakes and coupled variations in the electric and magnetic fields. In this set of eight reports in this issue, we report the first results from the seismological component of the MELT Experiment, which completed the data acquisition phase in May 1996. The electromagnetic data acquisition began at that time and was completed in June 1997.

Fifty-one ocean-bottom seismometers (OBSs) were deployed across the EPR in November 1995 in two linear arrays ~800 km long (Fig. 1). This site is in the middle of the longest, straightest section of the global spreading system and, with a total spreading rate of about 145 km per million years, it is one of the fastest spreading parts of the mid-ocean ridge system. This site thus provides an end-member test of the hypothesis that upwelling should be more linear at faster spreading rates, where theory indicates that passive flow is most likely to be dominant (*7*). Likely teleseismic earthquake sources are distributed at a wide range of azimuths, and the oceanic paths are relatively simple. We were fortunate to have a good distribution of large events during the 6-month recording period (Fig. 2), including some earthquakes at depths greater than 100 km. In the stable temperature environment of the sea floor, the seismometers (*13*) recorded signals with reliable phase and amplitude to a period of 50 s and greater, depending on the size of the earthquake. The best signal-to-noise ratio was typically in the 10- to 30-s band, which is a low-noise "window."

Each of the MELT reports in this issue describes results from different techniques to address issues of mantle flow and melt production. Geophysical mapping surveys (*14*) show that there is an asymmetry to the ridge in this area: the sea floor is subsiding more slowly on the Pacific Plate to the west than on the Nazca Plate to the east; the west side has a greater population of small seamounts; the Pacific Plate is moving almost twice as fast to the west as the Nazca Plate is moving to the east in the hot spot coordinate frame, causing the axis itself to migrate to the west; and, through a series of rapidly propagating rifts or overlapping spreading centers, the net accretion of new sea floor or half-spreading rate is more rapid on the Nazca Plate side, causing additional migration of the spreading center to the west. The asymmetry in subsidence and volcanic activity probably indicates a basic asymmetry in thermal structure and melt production.

An asymmetry in seismic structure across the ridge is clear in the pattern of *P* and *S* wave delays (*15*). The average gradient in delay time for *S* waves is about twice as large on the east side as on the west, roughly proportional to the difference in subsidence rates. Except for the station at the spreading center axis that is probably affected by melt in the crust, the most delayed *P* and *S* arrivals are displaced to the west of the axis. Like the body waves, the pattern of Rayleigh wave phase velocities is asymmetric. The velocities are low to the west of the axis and increase rapidly immediately to the east of the axis (*16*). Overall, the region of low velocities is several hundred kilometers across and is clearly not confined to a narrow region of concentrated upwelling predicted by some dynamic flow models.

There are at least two components of mantle structure contributing to the pattern of delays and asymmetry. Shear wave splitting measurements show that the mantle is anisotropic and that there is greater splitting to the west than to the east of the axis (*17*). This anisotropy contributes to the pattern; for example, delays for *S* waves polarized in the slow direction are more asymmetric than for those polarized in the fast direction (*15*). A second contributor to the delay pattern is variations in the amount of melt present in the upper mantle. The magnitude of the observed changes are too large to be due to the effect of velocity increases caused by solid-state cooling of the lithosphere and asthenosphere with increasing distance from the rise axis (*15*). The maps of phase velocities

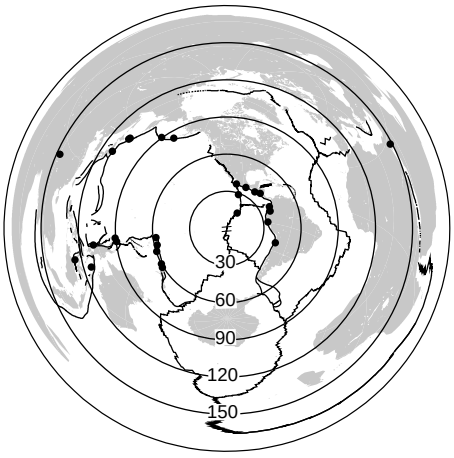

Fig. 2. Epicenters of earthquakes used as sources in the MELT Experiment. The location of OBS arrays are indicated by two short lines at the center of the map (azimuthal equidistant projection).

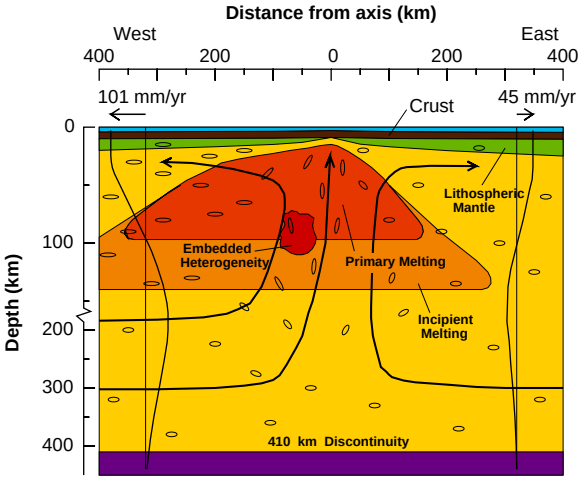

Fig. 3. Schematic cross-section of the East Pacific Rise at 17°S. The Pacific Plate, moving at 101 mm/year in the hot spot coordinate frame, is to the left in the diagram. The broad asymmetric region of low seismic velocities is interpreted to be the primary melt production region. The region labeled embedded heterogeneity represents additional melting created by anomalously enriched source material or localized upwelling; its dimensions are not well constrained. Although the exact flow pattern is not known, the faster motion of the Pacific Plate is expected to create greater shear in the upper mantle, inducing stronger anisotropy. The solid lines continuing down from velocity vectors indicate possible vertical profiles of horizontal velocities away from the ridge axis, with greater return flow coming from the west. The small ellipses represent the direction of preferred alignment of olivine a axes, with flatness increasing with increasing degree of alignment.

of 25-s Rayleigh waves show that there are large changes in velocity at depths of 15 to 70 km. This depth range is expected on the basis of petrological arguments (*9*) to be the primary melt production region, and the velocities in this depth range are so low that melt must be present (*16, 18*).

Return mantle flow toward the ridge (Fig. 3) from the Pacific Superswell region to the west (*19*) may bring in higher temperature asthenosphere that creates relatively slow subsidence and, coupled with the more rapid motion of the Pacific Plate, melting that continues farther off-axis. This off-axis melt may be augmented locally by the partial melting of embedded mantle heterogeneities (*16*). Less off-axis melting may occur on the east side where upwelling is slower and the mantle may already have been partially depleted by upwelling beneath the Pacific Plate.

The absolute magnitude of the velocity reduction due to the presence of melt depends on the shape of the melt pockets, but the ratio of *S* to *P* anomalies gives some information on shape. Spheroidal inclusions of melt cause about 2.3 times the delay for *S* waves compared with *P* waves; in the limit of randomly oriented thin films of melt, the ratio is about 3.9. The observed ratio near the axis is slightly greater than 3.0 (*15*), which is consistent with experimental observations of the distribution of the shapes of melt inclusions (*20*). The moderate attenuation of Rayleigh and *S* waves (*18*) also suggests that melts are not distributed primarily in thin films. For this distribution, *S* wave delays and Rayleigh wave velocity variations imply that the minimum melt concentration is 1 to 2% in the primary melt production region. Because the maximum degree of melting is expected to be about 20% (*21*), melt must be efficiently extracted from the mantle.

Modeling waveforms from regional events along the EPR to the north indicates that the lowest shear wave velocities, and probably the highest melt concentrations, extend to a depth of nearly 100 km (*18*). If there is a well-defined bottom to the low-velocity zone, it could be as deep as 150 km, although there may be instead a gradual transition extending to about 180 km. Tomographic experiments on modeling the *P* and *S* wave delays also demonstrate that lateral variations in structure within the array are required at depths exceeding 100 km (*15*). These observations suggest that the primary melt production in the upwelling mantle begins at about 100 km and that trace amounts of melting occur to depths of 150 km or more (Fig. 3). Our results thus support geochemical inferences that a significant amount of the melt production must occur in the garnet stability field at depths greater than 60 to 80 km (*10*).

A limit on the depth extent of anomalous structure is provided by *P*-to-*S* conversions at the primary seismic discontinuities 410 and 660 km below the surface. The time difference between conversions shows that the interval between 410 and 660 km is of normal thickness and that, therefore, significant temperature anomalies probably do not extend to 410 km (*22*). Waveform modeling of *S* waves from a regional event also indicates no anomalous structure in the 300- to 410-km depth range (*18*). These observations support the hypothesis that ridges passively tap the asthenosphere and do not represent buoyant, upwelling limbs of whole-mantle convection cells extending deep into the lower mantle.

Seismic anisotropy is usually caused by the systematic alignment of fluid-filled cracks or by lattice-preferred orientation of crystals, and both mechanisms probably contribute to the observed anisotropy. If melt-filled cracks were the dominant cause, however, we would expect that anisotropy would be greatest where the average velocities are lowest and that the alignment of cracks would make the fast direction parallel to the ridge. In contrast, we find that the fast direction for shear-wave splitting and Rayleigh waves is perpendicular to the ridge (*16, 17*), and that Rayleigh wave azimuthal anisotropy is least in the broad region of low velocities near the spreading center (*16*). Thus, seismic anisotropy is probably dominated by crystalline anisotropy. Anisotropy may be more pronounced beneath the Pacific Plate because there is greater shear caused by the faster motion of the Pacific Plate relative to the deep mantle and by the return flow in the asthenosphere toward the ridge (Fig. 3). The fast olivine a axis is tilted upward beneath the spreading center by the upwelling, then rotated more horizontally near the top of the upwelling region. Anisotropy in the lid immediately beneath the Mohorovicic discontinuity (the Moho) consistent with horizontal alignment of the a axis in the direction of spreading has been detected in the MELT study area by the splitting of *S* waves from local microearthquakes (*23*) and is suggested by anomalously high velocities of refracted *P* waves in the direction of spreading in the Pacific Plate (*24*).

The axial topographic high is broadest at about 17°15′ S, near where the primary OBS profile crosses the ridge (*14*). It systematically narrows northward up to a small overlapping spreading center (OSC) at 15°55′ S (Fig. 1). Gravity analysis shows that either the crust is thinner or there are increases in crust or mantle density in the vicinity of this OSC (*14*). Because this OSC might mark a boundary in mantle upwelling or melt production, the secondary OBS array (Fig. 1) was placed to cross the ridge just north of the OSC where the mantle Bouguer gravity anomaly reaches a maximum. Wide-angle seismic refraction data recorded on this secondary OBS array show that crustal thickness and structure near this small OSC is normal (*24, 25*). Therefore, the gravity anomaly probably is caused by denser and perhaps colder mantle near the OSC. *P* and *S* wave arrivals from teleseismic earthquakes are earlier along the secondary array than at comparable distances from the axis in the primary array, consistent with lower temperatures or lower melt fractions near the OSC (*15*). Finally, Rayleigh wave phase velocities show a pronounced, along-axis increase beginning in the vicinity of the OSC (*16*), suggesting that melt concentrations are lower beneath the OSC and northward.

One of the most surprising observations of the MELT Experiment is that the lowest velocities do not lie directly under the ridge axis. It is possible that anisotropy masks the low velocities to some extent (*15*), but the observation that *P* waves, *S* waves aligned both parallel and perpendicular to the ridge, and Rayleigh waves all detect a displacement of the center of the low velocities to the west suggests that the highest melt concentrations may be found beneath the Pacific Plate. The three-dimensionality detected by Rayleigh waves and body wave delays implies that there may be an off-axis center of upwelling and melt production that is dynamically driven and originates deep in the mantle. The association of isotopic anomalies with this section of the ridge (*26*) is consistent with a lower mantle origin, but these anomalies and the seismic observations are also consistent with anomalous melting of an embedded compositional heterogeneity within a passively upwelling mantle (Fig. 3). The efficient extraction of most of the melt from the mantle, the existence of short-lived uranium-series disequilibria in fresh mid-ocean ridge basalts (*27*), and the association of temporal variations in volcanism with melting of the ice cap on Iceland (*28*) all indicate that melt is removed in about 1000 years from a depth of 60 or 70 km. Thus, the melt concentrations we see today may not be representative of long-term melt productivity. Melt may simply be efficiently extracted from beneath the ridge, and melting of off-axis heterogeneities may produce local anomalies that persist for a limited period of time.

REFERENCES AND NOTES

1. R. S. Detrick *et al.*, *Nature* **326**, 35 (1987); E. E. Vera *et al.*, *J. Geophys. Res.* **95**, 15529 (1990).
2. M. Spiegelman and D. McKenzie, *Earth Planet. Sci.*

Lett. **83**, 137 (1987).
3. J. Phipps Morgan, *Geophys. Res. Lett.* **14**, 1238 (1987).
4. D. W. Sparks and E. M. Parmentier, *Earth Planet Sci. Lett.* **105**, 368 (1991).
5. D. McKenzie, *J. Petrol.* **25**, 713 (1984); N. M. Ribe, *Geophys. J. R. Astron. Soc.* **83**, 487 (1985); M. J. Daines and F. M. Richter, *Geophys. Res. Lett.* **15**, 1459 (1988).
6. W. Su and W. R. Buck, *J. Geophys. Res.* **98**, 12191 (1993).
7. E. M. Parmentier and J. Phipps Morgan, *Nature* **348**, 325 (1990).
8. X. Wang, J. R. Cochran, G. A. Barth, *J. Geophys. Res.* **101**, 17927 (1996); G. A. Barth and J. C. Mutter, *ibid.*, p. 17951.
9. P. C. Hess, in *Mantle Flow and Melt Generation at Mid Ocean Ridges*, J. Phipps-Morgan, D. K. Blackman, J. Sinton, Eds. (American Geophysical Union, Washington, DC, 1992), pp. 67–102.
10. V. J. M. Salters and S. R. Hart, *Nature* **342**, 420 (1989); P. D. Beattie, *ibid.* **363**, 63 (1993); R. S. White, D. McKenzie, R. K. O'Nions, *J. Geophys. Res.* **97**, 19683 (1992).
11. P. J. Wyllie, *J. Geophys. Res.* **76**, 1328 (1971).
12. W. J. Su, R. L. Woodward, A. M. Dziewonski, *Nature* **360**, 149 (1992).
13. Fifty of the 51 OBSs were equipped with three-component, 1-Hz seismometers (model L4C, Mark Products) as well as either a hydrophone or Cox-Webb differential pressure gauge (DPG) to record pressure variations. One was equipped only with a hydrophone. Several methods for deploying, leveling, filtering, and recording were used by four instrument groups. Data were recorded at either 16 or 32 samples per second, except during the seismic refraction phase of the experiment when higher rates were used. Instrument response characteristics were derived for each type of instrument and tested by comparing corrected waveforms of earthquakes at adjacent stations. The OBSs operated independently on battery power, and no data were transmitted back to the recording ship. After correction for clock drift, the timing errors are estimated to be less than 0.01 s. After reaching the sea floor, each OBS was located precisely by acoustically ranging to a transponder from the ship, which was navigated with the P-code Global Positioning System. Locations are estimated to be accurate within about 10 m. At the end of the experiment, acoustic signals were sent to release the weights (anchors) of each OBS. Fifty of the 51 OBSs were recovered. To reduce noise, in three of the four basic OBS designs we deployed the seismometer package separately from the recording package after reaching the sea floor. This mechanical deployment procedure was the most serious instrumental problem in the experiment. The seismometer package did not deploy properly at 20 sites. Seismic records from these OBSs were limited to the waves with pressure components, including *P* waves, *S*-to-*P* converted phases, and Rayleigh surface waves.
14. D. S. Scheirer, D. W. Forsyth, M.-H. Cormier, K. C. Macdonald, *Science* **280**, 1221 (1998).
15. D. R. Toomey *et al*., *ibid.*, p. 1224.
16. D. W. Forsyth, S. C. Webb, L. M. Dorman, Y. Shen, *ibid.*, p. 1235.
17. C. J. Wolfe and S. C. Solomon, *ibid.*, p. 1230.
18. S. C. Webb and D. W. Forsyth, *ibid.*, p. 1227.
19. M. K. McNutt and A. V. Judge, *ibid.* **248**, 969 (1990); J. Phipps Morgan, W. J. Morgan, Y.-S. Zhang, W. J. F. Smith, *J. Geophys. Res.* **100**, 12573 (1995).
20. U. H. Faul, D. R. Toomey, H. S. Waff, *Geophys. Res. Lett*. **21**, 29 (1994).
21. C. H. Langmuir, E. M. Klein, T. Plank, in (*9*), pp. 183–280.
22. Y. Shen, A. F. Sheehan, K. G. Dueker, C. de Groot-Hedlin, H. Gilbert, *Science* **280**, 1232 (1998).
23. S.-H. Hung and D. W. Forsyth, *Eos* **78**, F688 (1997).
24. S. Bazin *et al.*, *Geophys. Res. Lett.*, in press.
25. J. P. Canales, R. S. Detrick, S. Bazin, A. J. Harding, J. A. Orcutt, *Science* **280**, 1218 (1998).
26. J. J. Mahoney *et al*., *Earth Planet. Sci. Lett.* **121**, 173 (1994).
27. M. Spiegelman and T. Elliott, *ibid.* **118**, 1 (1993).
28. M. Jull and D. McKenzie, *J. Geophys. Res.* **101**, 21815 (1996).
29. W. H. F. Smith and D. T. Sandwell, *ibid.* **99**, 21803 (1994).
30. The MELT Experiment is part of the RIDGE (Ridge Inter-Disciplinary Global Experiments) program and is funded by NSF.

18 February 1998; accepted 21 April 1998

Off-Axis Crustal Thickness Across and Along the East Pacific Rise Within the MELT Area

J. Pablo Canales,* Robert S. Detrick, Sara Bazin, Alistair J. Harding, John A. Orcutt

Wide-angle seismic data along the Mantle Electromagnetic and Tomography (MELT) arrays show that the thickness of 0.5- to 1.5-million-year-old crust of the Nazca Plate is not resolvably different from that of the Pacific Plate, despite an asymmetry in depth and gravity across this portion of the East Pacific Rise. Crustal thickness on similarly aged crust on the Nazca plate near a magmatically robust part of the East Pacific Rise at 17°15′S is slightly thinner (5.1 to 5.7 kilometers) than at the 15°55′S overlapping spreading center (5.8 to 6.3 kilometers). This small north-south off-axis crustal thickness difference may reflect along-axis temporal variations in magma supply, whereas the across-axis asymmetry in depth and gravity must be caused by density variations in the underlying mantle.

The MELT area between 15° to 19°S (*1*–*7*) shows a pronounced asymmetry across the East Pacific Rise (EPR) in several characteristics such as spreading rate (faster to the east) (*5*, *8*), subsidence rate (slower on the west) (*6*), and gravity anomaly [a less pronounced increase of the mantle Bouguer anomaly (MBA) away from the ridge axis on the Pacific Plate than on the Nazca Plate] (*7*). This asymmetry in MBA across the EPR in the MELT area can be interpreted in terms of variations in crustal thickness or in crustal or mantle density. The lower MBA and shallower seafloor on the Pacific Plate ~100 km west of the rise axis (*7*) could mean that the oceanic crust is ~1 km thicker than similarly aged crust east of the rise axis or that the mantle there is hotter and less dense (*9*). We used wide-angle seismic data collected as part of the MELT experiment to determine the crustal thickness variations across and along the EPR to evaluate the crustal contribution to the asymmetry in regional depth and gravity anomalies across the EPR in this area.

The data were recorded by 15 ocean-bottom seismometers (OBS) (*10*) deployed along three seismic refraction lines (Fig. 1). The northern line along the secondary MELT array was 360 km long and crossed the EPR a few kilometers north of the 15°55′S overlapping spreading center (OSC), and included five instruments (OBS sites 3, 4, 5, 7, and 8) spaced 40 to 90 km apart (hereafter referred to as line 1). Ten instruments were deployed along the primary MELT array, which intersects the rise axis near 17°15′S where a shallow and robust axial high is present (*7*). Four of these instruments (OBS sites 21, 23, 24, and 26), spaced 15 to 50 km apart, were located on the Nazca Plate along a line ~160 km in length (line 2). The remaining six instruments (OBS sites 39, 40, 42, 43, 45, and 46), spaced 15 to 80 km apart, were located on the Pacific Plate along a line ~230 km in length (line 3).

The seismic source for this experiment was a 4450-in^3 airgun array aboard the R/V *Melville* fired at a 100-s repetition rate. All of the OBS record sections showed clear crustal refractions (Pg arrivals) and Moho reflections (PmP arrivals); upper mantle refractions (Pn arrivals) were observed on some of the receivers (Table 1). The selected picks were analyzed by ray trace modeling (*11*). We determined the crustal velocity structure from Pg arrivals of diving waves turning up to ~3.0 to 3.5 km below the seafloor (Fig. 2). Despite some differences along each profile, the data showed that the top of the crust consists of a layer ~200 m thick in which the velocities increase from 2.5 to 4.0 km/s. These velocities are not directly constrained by turning rays in the uppermost crust, but this combination of velocity and thickness is required to match the delay of the Pg arrivals at the smallest shot-receiver ranges. Below this layer, crustal velocities increase from 4.0 to 7.0 km/s at a sub-seafloor depth of 3.0 to

J. P. Canales and R. S. Detrick, Department of Geology and Geophysics, Woods Hole Oceanographic Institution, 360 Woods Hole Road, Woods Hole, MA 02543, USA. S. Bazin, A. J. Harding, J. A. Orcutt, Institute of Geophysics and Planetary Physics, Scripps Institution of Oceanography, University of California San Diego, La Jolla, CA 92093–0225, USA.

*To whom correspondence should be addressed. E-mail: juan@sienna.whoi.edu